

Isoscalar and isovector transition amplitudes in  $A = 13$

R. J. Peterson, J. R. Shepard, and R. A. Emigh

*Nuclear Physics Laboratory, University of Colorado, Boulder, Colorado 80309*

(Received 13 April 1981)

Data for the isovector charge exchange reaction ( ${}^3\text{He},t$ ) on  ${}^{13}\text{C}$  are compared to  ${}^3\text{He}$  inelastic scattering data containing both isovector and isoscalar parts, and to strictly isoscalar inelastic  ${}^4\text{He}$  scattering to determine the ratio of  $\Delta T = 1$  to  $\Delta T = 0$  transition amplitudes for several states. These amplitudes are used to compute the charge asymmetry for  $\pi^+$  and  $\pi^-$  inelastic scattering on  ${}^{13}\text{C}$  and good agreement is found for six excited states. A ratio of mirror electromagnetic reduced transition rates is also correctly predicted. Several scattering mechanism models are compared for the excitation of the high-spin  $7/2^+$  and  $9/2^+$  states of  ${}^{13}\text{C}$  or  ${}^{13}\text{N}$  but no single mechanism can be shown to dominate.

$$\left[ \begin{array}{l} \text{NUCLEAR REACTIONS } {}^{13}\text{C}({}^3\text{He},{}^3\text{He}')({}^3\text{He},t)({}^4\text{He},{}^4\text{He}') E_{3\text{He}} \\ = 43.6 \text{ MeV}, E_\alpha = 35.5 \text{ MeV}; \text{ measured } \sigma(E,\theta), \text{ deduce ratio of iso-} \\ \text{vector to isoscalar transition amplitude.} \end{array} \right]$$

I. INTRODUCTION

A striking isospin asymmetry is seen in comparisons of  $\pi^+$  and  $\pi^-$  inelastic scattering on  ${}^{13}\text{C}$ .<sup>1-3</sup> These results are a consequence of the coherent mixture of isoscalar ( $\Delta T = 0$ ) and isovector ( $\Delta T = 1$ ) amplitudes for transitions between initial and final nuclear states of isospin  $\frac{1}{2}$ . Perhaps the most noteworthy excitation is that of a  $\frac{9}{2}^+$  state at 9.50 MeV which is essentially of a pure neutron nature, with perfect mixing of the isoscalar and isovector modes.

In the present study, the inelastic scatterings of  ${}^3\text{He}$  and  ${}^4\text{He}$  by  ${}^{13}\text{C}$  will excite the same states as seen in pion scattering and the ( ${}^3\text{He},t$ ) reaction will excite their analogs with an isovector amplitude. Comparisons of these results may be cast in the form of ratios of isovector to isoscalar reduced matrix elements for each transition. In this manner the conclusions drawn from the analysis of the pion data can be directly compared to conventional low-energy light-ion reaction data.

This same ratio of isovector to isoscalar reduced matrix elements may be obtained from comparisons of electromagnetic decay rates of excited states in analog nuclei<sup>4-6</sup> and by comparisons of proton to neutron<sup>7-9</sup> or triton to  ${}^3\text{He}$  inelastic scattering cross sections.<sup>10</sup> Although the isoscalar amplitude is expected to dominate the collective excitations,<sup>11</sup> the isovector amplitude is more state dependent.<sup>12</sup>

Thus, these several probes together can offer valuable new information on nuclear structure.<sup>13</sup>

The feature exploited for all these scatterings is the different relative phase and magnitude for isovector and isoscalar excitations, depending on the isospin projection of the projectile through the Wigner-Eckart theorem applied to the projectile and nuclear isospin coordinates.

One of the assumptions that must be made for this analysis is the true identity of all features of analog states in  ${}^{13}\text{C}$  and  ${}^{13}\text{N}$ . The projectile coordinates, the isospin features in particular, must be separable from the nuclear coordinates and the distortions due to differing optical potentials for outgoing  ${}^3\text{He}$  or  $t$  are assumed to be the same.

The Wigner-Eckhart theorem for the transition between projectile and nuclear isospin states is used in the form<sup>14</sup>

$$\begin{aligned} &\langle T_1 T_{1z} | M_{\Delta T \Delta T_z} | T_2 T_{2z} \rangle \\ &= M_{\Delta T} (-1)^{T_1 - T_{1z}} \begin{bmatrix} T_1 & \Delta T & T_2 \\ -T_{1z} & \Delta T & T_{2z} \end{bmatrix}, \end{aligned}$$

with reduced matrix elements  $M_0$  and  $M_1$ . The coefficients for each transition, reduced in both projectile and nuclear isospin coordinates, are listed in Table I. The nuclear reduced matrix elements for  $\Delta T = 1$  are multiplied by  $\sqrt{3}$  to form the ratios listed below. This provides more familiar equations for the scattering reactions.

TABLE I. Coefficients of the projectile and nucleon reduced matrix elements are listed. A factor of  $\sqrt{3}$  has multiplied the  $\Delta T = 1$  nuclear reduced matrix element to define the  $M_1$  used in the text.

Projectile	$\Delta T = 0$	$\Delta T = 1$	
$({}^3\text{He}, t)$	0	$+\frac{1}{\sqrt{3}}$	
$({}^3\text{He}, {}^3\text{He}')$	$\frac{1}{\sqrt{2}}$	$-\frac{1}{\sqrt{6}}$	
$(t, t')$	$-\frac{1}{\sqrt{2}}$	$-\frac{1}{\sqrt{6}}$	
$(\alpha, \alpha')$	+1	0	
$(\pi^+, \pi^+')$	$-\frac{1}{\sqrt{3}}$	$\frac{1}{\sqrt{6}}$	(one step)
	$-\sqrt{8/9}$	$\sqrt{2/9}$	(two step)
$(\pi^-, \pi^-')$	$\frac{1}{\sqrt{3}}$	$\frac{1}{\sqrt{6}}$	(one step)
	$\sqrt{8/9}$	$\sqrt{2/9}$	(two step)
Photon	$\frac{1}{\sqrt{2}}$	$-\frac{1}{\sqrt{2}}$	
Nuclear			
${}^{13}\text{C} \rightarrow {}^{13}\text{C}$	$\frac{1}{\sqrt{2}}$	$\frac{1}{\sqrt{2}}$	
${}^{13}\text{C} \rightarrow {}^{13}\text{N}$	0	-1	
${}^{13}\text{N} \rightarrow {}^{13}\text{N}$	$-\frac{1}{\sqrt{2}}$	$\frac{1}{\sqrt{2}}$	

For mass three beams, the ratios of cross sections are then simply

$$\frac{d\sigma({}^3\text{He}, t)}{d\sigma({}^3\text{He}, {}^3\text{He}')} = 2 \left| \frac{M_1}{M - \sqrt{3}M} \right|^2,$$

$$\frac{d\sigma(t, t')}{d\sigma({}^3\text{He}, {}^3\text{He}')} = \left| \frac{M_1 + \sqrt{3}M_0}{M_1 - \sqrt{3}M_0} \right|^2.$$

The strictly isoscalar scattering of  ${}^4\text{He}$  can be included in the analysis only after corrections for differing beam energies and optical potential distortions; at the beam energies selected for this study the wave numbers for the  ${}^3\text{He}$  and  ${}^4\text{He}$  data are identical. The corrections needed to relate the  ${}^3\text{He}$  and  ${}^4\text{He}$  data are made by comparing both to collective DWBA predictions to give deformations  $\beta$  for each transition. The ratio of these deformations is taken to represent the ratio of cross sections. This procedure is clearly more dependent upon the reaction model than is the comparison of  ${}^3\text{He}$  charge exchange and scattering. The ratio is

$$\frac{\beta^2(\alpha, \alpha')}{\beta^2({}^3\text{He}, {}^3\text{He}')} = 6 \left| \frac{M_0}{M_1 - \sqrt{3}M_0} \right|^2.$$

This comparison will be used for all states, even for clearly noncollective excitations. Odd-mass  ${}^{13}\text{C}$  permits natural parity excitations of all states, consistent with this collective model for the scattering, which compares only  $\Delta S = 0$  terms. Although the interactions may be noncentral or spin dependent for the  ${}^3\text{He}$ , both  ${}^3\text{He}$  and  ${}^4\text{He}$  have interaction ranges and mean free paths short compared to nuclear radii and hence the different interactions may be of minor importance. The results to be presented below will demonstrate that this is indeed the case.

This set of ratios involving only  $M_0$  and  $M_1$  allows the ratio of isovector to isoscalar nuclear reduced transition matrix elements to be determined in  ${}^3\text{He}$ -induced reactions, and with the alpha particle data, even the choice of sign allowed when square roots are taken is removed. The comparisons in Ref. 6 do not examine the possibility of two roots.

The isovector and isoscalar reduced electromagnetic transition rates interfere with opposite signs for the two members of the  $A = 13$  mirror pair,<sup>4</sup> with

$$\frac{B(EL)({}^{13}\text{N})}{B(EL)({}^{13}\text{C})} = \left| \frac{M_0 + M_1}{M_0 - M_1} \right|^2.$$

The electromagnetic transition certainly differs greatly from that induced by the  ${}^3\text{He}$  or  ${}^4\text{He}$ , and only the isospin features are correctly included in the expression above. Since the multipole operator is of the form  $r^L$  the surface of the nucleus is heavily weighted and we hypothesize that the ratios of transition strengths can be compared with the same relative importance for  $M_0$  and  $M_1$  as found for the strongly absorbed helium ions.

The collective Lane model has been used for comparison of proton and neutron transition strengths and for a comparison to electromagnetic transition strengths, of equal isoscalar and isovector sensitivity.<sup>7,8</sup> Collective strengths differing by as much as 20% were analyzed. This completely collective approach is not followed in the present work because the greatest differences between charge exchange and inelastic scattering are found for weakly excited states, not the more collective levels.

The sensitivity of inelastic pion scattering data to differing neutron and proton amplitudes has been examined in this collective model<sup>9</sup> for the lowest  $2^+$  states of  ${}^{24}\text{Mg}$  and  ${}^{152}\text{Sm}$ . The effects noted in  ${}^{13}\text{C}$  are much stronger for some states than anticipated

from this strictly collective picture where only a factor of  $(N - Z)/A \sim 0.08$  determines the ratio of isovector to isoscalar matrix elements.

Pion scattering data may be used to obtain pion transition amplitudes  $P_0$  and  $P_1$  analogous to the isoscalar and isovector amplitudes  $M_0$  and  $M_1$ . Formation and decay of an intermediate nucleon isobar is required for the scattering to include the dominant 3-3 resonance. For this mechanism,<sup>5,15</sup>

$$\frac{d\sigma(\pi^-)}{d\sigma(\pi^+)} = \left| \frac{P_1 + 2P_0}{P_1 - 2P_0} \right|^2.$$

For a purely neutron nuclear excitation, these equations reduce to the familiar nine to one  $\pi^-$  to  $\pi^+$  ratio and a vanishing electromagnetic transition in  $^{13}\text{C}$ .<sup>4</sup>

If a truly similar and separable scattering mechanism is responsible for the pion data, the ratio of reduced matrix elements  $P$  may be replaced by the ratio of reduced matrix elements  $M$ , and the asymmetry between positive and negative pion scattering can be predicted. The inclusion of alpha particle scattering data removes the ambiguity encountered in this comparison. The short range of the hadronic probes may allow this comparison in spite of the problems that could be encountered in principle because of dynamical differences in the reaction mechanisms. The test of this hypothesis is the subject of this work.

There are several instances of good agreement between pionic and electromagnetic transition amplitudes,<sup>5,6,16</sup> and it is the purpose of the present study to include baryonic excitations in this comparison. In addition to the simple ratios of matrix elements, specific reaction model calculations are made for some transitions in  $A = 13$ . Some relevant data from single-nucleon transfer data are presented and used to determine the nature of the microscopic wave functions used in these analyses.

## II. EXPERIMENTAL AND THEORETICAL METHODS

The  $^3\text{He}$  scattering and charge exchange data were obtained during the same run on the same 99.4% enriched  $^{13}\text{C}$  target. The University of Colorado AVF cyclotron provided the beam of 43.6 MeV  $^3\text{He}$ , and the reaction products were analyzed with the beam swinger magnetic spectrograph.<sup>17</sup> An energy resolution of 35 keV was obtained for sharp final states. Sample spectra are shown as Figs. 1–3; all compiled states<sup>18</sup> in the excitation re-

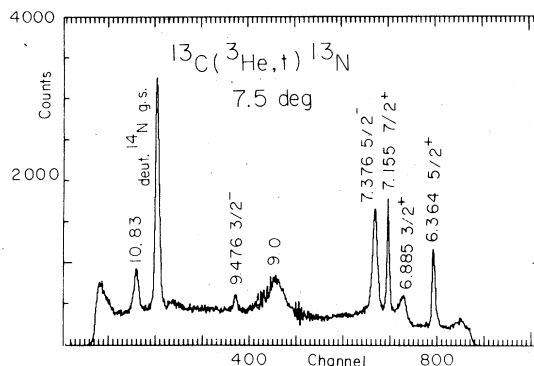


FIG. 1. A sample  $(^3\text{He},t)$  spectrum on  $^{13}\text{C}$ . Known states are labeled, with the 9.0 MeV broad peak containing the  $\frac{9}{2}^+$  state. The jiggle in the spectrum near channel 500 is an artifact in the detector response.

gions examined were noted.

Absolute cross sections were determined by comparisons of small angle elastic scattering data to optical model predictions for an estimated accuracy of  $\pm 12\%$ , and agreed with those measured at a similar beam energy for the stronger states by solid-state counters.<sup>19</sup> The relative cross sections for ejected tritons and  $^3\text{He}$  are known to an accuracy of  $\pm 5\%$ , added in quadrature to the statistical uncertainty. The energy calibration was very clearly defined by the strong deuteron peaks seen in spectra obtained simultaneously without particle identification. The data for the  $^{13}\text{C}(^3\text{He},d)^{14}\text{N}$  reaction have been analyzed and published separately,<sup>20</sup> and provide input for two-step calculations with sequential nucleon transfer, to be discussed in Sec. IV.

The magnetic spectrograph momentum spectra for the tritons were sometimes obscured at critical

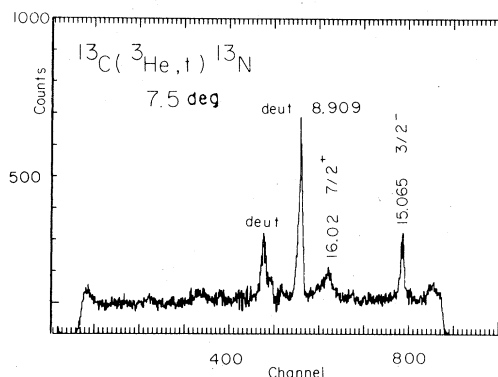


FIG. 2. A high excitation spectrum of the levels of  $^{13}\text{N}$ , showing that only two states are populated in this region. The deuteron peaks result from imperfect particle identification, and serve as excellent calibration points.

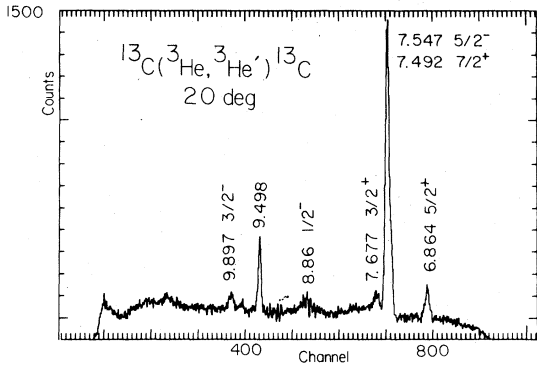


FIG. 3. A sample  $^3\text{He}$  inelastic scattering spectrum on  $^{13}\text{C}$  showing the 9.498 MeV  $\frac{9}{2}^+$  state.

regions by the intense deuteron groups. An auxiliary experiment was carried out with solid-state detectors to avoid this problem, since the deuteron groups obscured other regions in the energy spectra. Some  $^3\text{He}$  inelastic scattering data were obtained simultaneously, providing reassurance on the relative strengths. In addition, the  $(^3\text{He},\alpha)$  reaction was studied to provide data to check two-step mechanisms, as described in Sec. IV.

The alpha particle scattering experiment was performed at 35.5 MeV with a single silicon solid state detector. An overall resolution of 65 keV was obtained, and a sample spectrum is shown as Fig. 4. The cross sections were determined to an accuracy estimated to be  $\pm 12\%$ .

Although the heart of the analysis is the simple ratio of cross sections, distorted wave Born approximation (DWBA) calculations are also carried out for corrections for charge,  $Q$ -value, and other dynamical differences among the reactions studied. These were also used to assess the dependence on the nucleon binding energies in  $^{13}\text{C}$  and  $^{13}\text{N}$ .

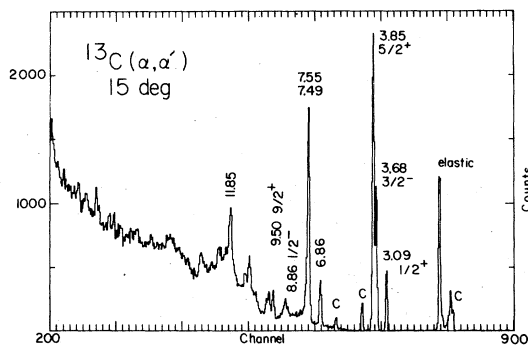


FIG. 4. A sample spectrum of  $^4\text{He}$  inelastic scattering from  $^{13}\text{C}$  at 35.5 MeV. A silicon solid state detector was used for these data.

Several sets of optical model and bound state parameters were examined; the one used here is from a recent study of elastic  $^3\text{He}$  scattering on light nuclei.<sup>21</sup> The same  $^4\text{He}$  optical parameters<sup>22</sup> were used for inelastic scattering and for the two-step calculations. The bound state for the nucleon involved in the pickup or stripping transition was determined by a thorough study of the  $^{12}\text{C}(^3\text{He},d)^{13}\text{N}$  reaction, with the parameters selected to give the proper single-nucleon spectroscopic factors.<sup>23</sup> Those parameters are listed in Table II.

In the microscopic inelastic DWBA calculations, a central Yukawa interaction of range 1 fm was used. Only the simplest shell model promotions were considered. In some cases a tensor interaction of inverse range  $0.7 \text{ fm}^{-1}$  was also used. All calculations were performed with the code DWUCK4.<sup>24</sup> The active nucleons were considered to be slightly bound, even when the actual final state was unbound. The sensitivity of the calculations to the binding energy is investigated below for several transitions.

All collective DWBA cross sections were computed with a simple first derivative form factor, even for  $\Delta L = 0$  and  $\Delta L = 1$  transitions where this cannot be valid. However, these calculations are intended only to correct the  $^4\text{He}$  data for comparison to the  $^3\text{He}$  data. The predicted shapes do not differ greatly from those with more realistic form factors.

### III. RESULTS

#### A. Ground states

The analog nature of the ground states of  $^{13}\text{C}$  and  $^{13}\text{N}$  cannot be exploited to extract ratios of matrix elements  $M_0$  and  $M_1$ , because of the elastic scattering nature of one of the transitions. On the other hand, the charge exchange data can be used for a test of the DWBA methods because of the simple

TABLE II. Optical model and bound state parameters used for the DWBA and CCBA analyses.

	$^3\text{He}, t$	$^4\text{He}$	Bound $n, p$	
$V$	-106.5	-216.8		MeV
$r_r$	1.15	1.30	1.30	fm
$a_r$	0.80	0.58	0.65	fm
$W_V$		-28.05		MeV
$4W_D$	55.48			MeV
$r_I$	1.25	1.50		fm
$a_I$	0.80	0.32		fm
$\lambda$			25.0	Thomas

analog, bound-state nature of the ground state of  $^{13}\text{N}$ . The data are shown in Fig. 5. Comparison to the collective DWBA prediction, with a form factor given by the derivative of the optical potentials, shows the clear  $\Delta L = 0$  angular dependence expected. A value of  $|\beta|$  equal to 0.061 is obtained from this comparison; with only one cross section the sign cannot be determined. Another choice of optical parameters provides a value 15% smaller.

### B. The $\frac{1}{2}^+$ states

The data to the analog  $\frac{1}{2}^+$  states at 3.09 MeV in  $^{13}\text{C}$  and 2.37 MeV in  $^{13}\text{N}$  are shown in Fig. 6; the collective  $\Delta L = 1$  DWBA predictions are shown as the solid curves. The ratio of charge exchange to scattering cross section is  $R = 0.097 \pm 0.02$ , with values of  $|\beta| = 0.11$  for  $^{13}\text{C}$  and  $|\beta| = 0.035$  for  $^{13}\text{N}$ . Differences in  $Q$  value and final charge produce no more than a 5% correction to the ratio of yields in the collective model. The dotted curves show the microscopic  $\Delta L = 1, \Delta S = 0$  DWBA predictions for promoting the valence  $p_{1/2}$  nucleon into the empty  $2s_{1/2}$  shell. The strength parameters giving the fits shown are  $V_0 = 101$  and  $V_\tau = 32$  MeV. The effects of the different binding energies in  $^{13}\text{C}$  and  $^{13}\text{N}$  are included in these calculations. The ratio of transition strengths is the same when guided by either the collective or microscopic DWBA predictions and indicates the expected isoscalar dominance.

The ratio  $R = 0.097$  for  $(^3\text{He}, t)$  to  $(^3\text{He}, ^3\text{He}')$  cross sections provides two solutions for the ratio of reduced matrix elements,  $M_1/M_0 = 0.23$  and  $-0.31$ . When used for the pionic ratio in the equation of Sec. I, predictions for the pion asymmetry are made:

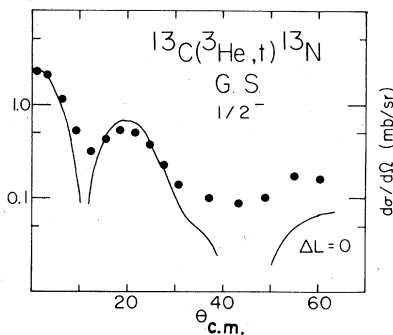


FIG. 5. The  $^{13}\text{C}(^3\text{He}, t)^{13}\text{N}$  ground state data are compared to a collective  $\Delta L = 0$  DWBA prediction.

$$A = \frac{d\sigma(\pi^-) - d\sigma(\pi^+)}{d\sigma(\pi^-) + d\sigma(\pi^+)} = \frac{4M_1M_0}{M_1^2 + 4M_0^2} = 0.23 \text{ or } -0.30.$$

This ambiguity can be resolved through the alpha particle scattering data. The data and DWBA fit for  $\beta = 0.19$  are shown in Fig. 7. The collective form factor is used for both the  $^3\text{He}$  and  $^4\text{He}$  calculations, and the ratio of  $^4\text{He}$  to  $^3\text{He}$  cross sections, corrected for the different reaction dynamics, is taken to be the ratios of the squares of the deformations  $\beta$ , and is equal to 2.76. The ratios of matrix elements 0.23 and  $-0.31$  from the  $(^3\text{He}, ^3\text{He}')$  and  $(^3\text{He}, t)$  work predict this cross section ratio to be 2.65 and 1.44, respectively. This comparison clearly selects the positive ratio of reduced matrix elements, which in turn predicts  $A_\pi = 0.23$ .

The pion scattering data of Dehnhard *et al.*<sup>1</sup> give  $A = 0.32 \pm 0.08$ , in agreement with the prediction from the present work, also for the positive ratio. The uncertainties involved in this analysis will be treated in a later section. These numerical results are summarized in Table III.

Two analog electromagnetic lifetimes are known for  $^{13}\text{C}$  and  $^{13}\text{N}$ .<sup>18</sup> When corrected for the decay energies the  $B(E1)$  reduced transition rates for the lowest  $\frac{1}{2}^+$  states of  $^{13}\text{N}$  and  $^{13}\text{C}$  are in the ratio of  $3.31 \pm 0.48$ . The ratios of matrix elements discussed above,  $-0.31$  and  $0.23$ , predict transition rates in the ratio 0.39 or 3.60, respectively. This latter choice agrees well with the data and selects the same solution as does the  $^4\text{He}$  scattering data and pion asymmetry results.

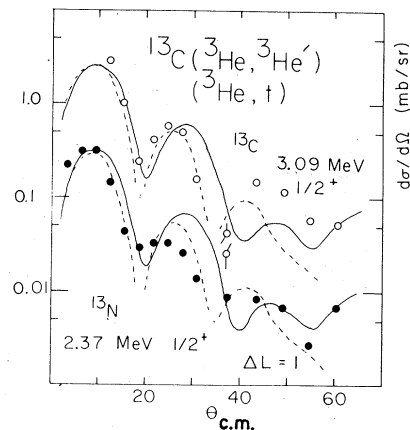


FIG. 6. Scattering and charge exchange data to the lowest  $\frac{1}{2}^+$  states are compared to collective  $\Delta L = 1$  DWBA predictions as the solid curves, and to broken  $\Delta L = 1$  microscopic DWBA predictions. The parameters are described in the text.

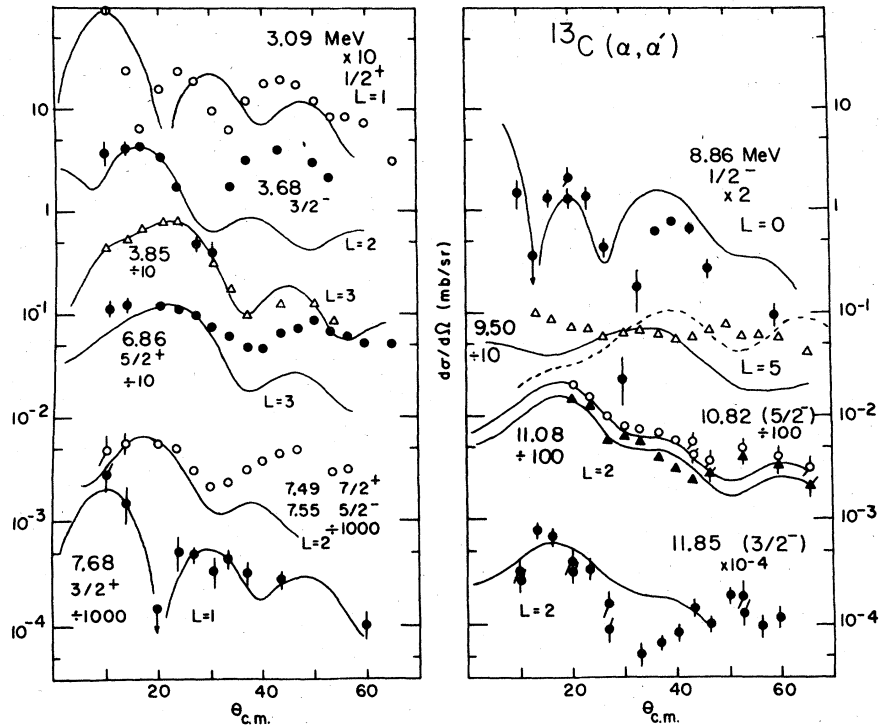


FIG. 7. Differential cross sections for levels of  $^{13}\text{C}$  excited by inelastic  $^4\text{He}$  scattering are compared to collective DWBA predictions as the solid curves. The broken curve for the 9.50 MeV state shows a prediction for sequential  $\beta_2$  and  $\beta_3$  excitation, multiplied by 5 for better comparison to the data.

### C. The first $\frac{3}{2}^-$ and $\frac{5}{2}^+$ states

The 3.51 MeV ( $\frac{3}{2}^-$ ) and 3.55 MeV ( $\frac{5}{2}^+$ ) states in  $^{13}\text{N}$  could not be separated, and so only the sum of the  $^{13}\text{C}$  cross sections can be compared. The  $^3\text{He}$  scattering data are shown in Fig. 8, compared to collective DWBA predictions for  $\Delta L = 2$  and 3 for the scattering data. This comparison provides  $\beta_2 = 0.166$  and  $\beta_3 = 0.172$ . The  $\Delta L = 3$  microscopic prediction for a pure promotion to the  $d \frac{5}{2}$  shell requires a normalization  $V_0 = 58$  MeV, assuming a strictly isoscalar excitation without spin transfer.

Since the ( $^3\text{He}, t$ ) data are for the unresolved doublet the sum of  $^3\text{He}$  scattering cross sections to the analog states is used to extract ratios of reduced matrix elements. The ratio of cross sections,  $0.23 \pm 0.02$ , predicts pion asymmetries of  $-0.51$  and  $0.33$ ; the second of these values is in agreement with the measured value of  $0.4 \pm 0.1$  for the unresolved doublet seen in pion scattering.<sup>1</sup> We may also use the ratio of  $^4\text{He}$  to  $^3\text{He}$  scattering data to the resolved states to make this prediction. The  $^4\text{He}$  data and DWBA fits appear in Fig. 7, with deformations  $\beta$  given in Table III. For the 3.68 MeV  $\frac{3}{2}^-$  state the scattering ratios predict pion asym-

metries of  $-0.63$  and  $0.78$ , while the 3.85 MeV  $\frac{5}{2}^+$  data predict  $0.36$  and  $0.91$ . Since the observed pion asymmetry of  $0.4 \pm 0.1$  is for the unresolved doublet, little can be said about this comparison until pion data of better resolution are available or unless the pion asymmetry depends upon the scattering angle, so that  $\Delta L = 2$  or  $\Delta L = 3$  contributions can be separated. The mirror ground state gamma transitions in  $^{13}\text{N}$  and  $^{13}\text{C}$  from the  $\frac{3}{2}^-$  states have known widths,<sup>18</sup> but an unknown mixture of  $E2$  and  $M1$  amplitudes. The resolved scattering cross sections to this state for  $^3\text{He}$  and  $^4\text{He}$  provide ratios  $M_1/M_0 = 4.1$  and  $-0.66$ , predicting the  $^{13}\text{N}$   $B(E2)$  to be either 2.69 or 0.04 times that for  $^{13}\text{C}$ . If the photon transition were only  $E2$ , the ratio of widths provides  $1.64 \pm 0.2$  for this comparison. The lack of agreement is not surprising, since  $M1$  decay is also to be expected.

### D. The first $\frac{3}{2}^+$ and second $\frac{5}{2}^+$ states

The 6.86 MeV  $\frac{5}{2}^+$  and 7.68 MeV  $\frac{3}{2}^+$  states in  $^{13}\text{C}$  and the 6.36 MeV  $\frac{5}{2}^+$  and 6.89 MeV  $\frac{3}{2}^+$  states in  $^{13}\text{N}$  are appreciably weaker than the first  $\frac{5}{2}^+$  states. The  $^3\text{He}$  data are shown in Fig. 9, with

TABLE III. Cross sections for  ${}^3\text{He}$  and  ${}^4\text{He}$  inelastic scattering and  $({}^3\text{He},t)$  charge exchange are summarized as the deformations  $\beta$ . The ratios of  $({}^3\text{He},t)$  to  $({}^3\text{He},{}^3\text{He}')$  cross sections yield two values for the ratio  $M_1/M_0$  of nuclear reduced matrix elements. These lead to predictions of the charge asymmetry in pion scattering to compare with the data of Dehnhard *et al.*<sup>b</sup>

States		$J^\pi$	$({}^3\text{He},{}^3\text{He}')$	$\beta_L$		$\alpha\alpha'$	$\frac{d\sigma({}^3\text{He},t)}{d\sigma({}^3\text{He},{}^3\text{He}')}$
${}^{13}\text{C}$	${}^{13}\text{N}$			$({}^3\text{He},t)$	$\alpha\alpha'$		
0	0	$\frac{1}{2}^-$		0.061			
3.09	2.37	$\frac{1}{2}^+$	0.113	0.035	0.19	0.097	
3.68	3.51	$\frac{3}{2}^-$	0.166		0.17		0.23
3.85	3.55	$\frac{5}{2}^+$	0.172		0.31		
6.86	6.36	$\frac{5}{2}^+$	0.055	0.041	0.042	0.59	
7.68	6.88	$\frac{3}{2}^+$	0.065	0.025	0.097	0.151	
7.49	7.16	$\frac{7}{2}^+$		0.060			0.17
7.55	7.38	$\frac{5}{2}^-$		0.056			
8.86	8.92	$\frac{1}{2}^-$	0.050		0.10		
9.50	9.0	$\frac{9}{2}^+$	0.072	0.083	0.16	2.0	
10.8	10.36	$\frac{5}{2}^-, \frac{7}{2}^-$	0.035	0.019	0.18	0.3	
11.08	10.83	$(\frac{1}{2}^-)^c$	0.046	0.037	0.15	1.4	
11.85	11.80	$(\frac{3}{2}^-)$	0.12	0.20	0.35	2.4	
15.11	15.07	$\frac{3}{2}^-, \frac{3}{2}^+$	0.065	0.065		1.0	
16.0	16.02	$\frac{7}{2}^+$	0.062	0.094	<0.1	1.4	

<sup>a</sup>Predicted pion asymmetry results with the positive square root of the charge exchange to scattering ratio used for the result listed first.

<sup>b</sup>Reference 1.

<sup>c</sup>The  $\Delta L = 2$  angular distributions seen in the present work imply a spin of  $\frac{3}{2}^-$  or  $\frac{5}{2}^-$ .

solid DWBA predictions for  $\Delta L = 3$  and 1, and the  ${}^4\text{He}$  data are shown in Fig. 7. The collective  $\beta$  values are listed in Table III; no microscopic DWBA calculations were performed. The ratios listed in Table III provide predictions for the pion asymmetry, but no data are available. An unexpected rise at small angles is seen for the charge exchange data to the 6.86 MeV  $\frac{5}{2}^+$  state; this may indicate a contribution due to  $\Delta L = 1$ ,  $\Delta S = 1$ , and  $\Delta J = 2$ .

The  ${}^4\text{He}$  scattering data is used as a consistency check of the isospin relations for these two states. For the 6.86 MeV  $\frac{5}{2}^+$  state, the ratio of  ${}^4\text{He}$  to  ${}^3\text{He}$  scattering yields is 0.585, while the ratios predicted from the ratios of reduced matrix elements obtained

from the  ${}^3\text{He}$  scattering and charge exchange data are 0.78 and 3.8. Neither is in close agreement with the  ${}^4\text{He}$  data. Strong multistep processes are indicated by the back angle  ${}^4\text{He}$  data, and if the reaction mechanisms are very different for  ${}^3\text{He}$  and  ${}^4\text{He}$  projectiles, the simple ratio arguments cannot work.

For the 7.68 MeV  $\frac{3}{2}^+$  state, which also shows extra  ${}^4\text{He}$  scattering strength at back angles, the  ${}^4\text{He}$  to  ${}^3\text{He}$  ratio of yields is 2.23, in contrast to predictions of 1.3 and 2.8 from the  ${}^3\text{He}$  scattering and charge exchange data.

#### E. The $\frac{7}{2}^+$ and $\frac{5}{2}^-$ states

<sup>a</sup>The 7.492 MeV  $\frac{7}{2}^+$  and 7.547 MeV  $\frac{5}{2}^-$  levels of  ${}^{13}\text{C}$  were not resolved in either inelastic scattering

TABLE III. (Continued).

$M_1/M_0$	Pion asymmetry		$\frac{d\sigma(\pi\pi')}{d\sigma(^3\text{He}, ^3\text{He}')}_{\text{Predicted}}$
	Predicted <sup>a</sup>	Observed <sup>b</sup>	
-0.31,0.23	-0.30,0.23	$0.32 \pm 0.08$	0.55,1.69
-0.55,0.34	-0.51,0.33	$0.4 \pm 0.1$	4.18,0.72
-1.03,0.47	-0.81,0.45		12.5,2.40
-0.41,0.28	-0.40,0.27		0.065,3.04
-0.44,0.20	-0.62,0.37	$-0.3 \pm 0.1$	0.38,1.92
		$0.2 \pm 0.1$	
-4.18,0.72	-0.78,0.64	$0.8 \pm 0.2$	0.17,5.84
-0.65,0.37	0.59,0.36		0.21,2.38
-1.17,0.50	-0.87,0.47		0.04,0.21
6.0,0.76	-0.60,0.66	$-0.1 \pm 0.05$	0.30,6.50
	0		1.0
-2.5,0.64	-0.97,0.58	$-0.6 \pm 0.2$	0.03,4.7

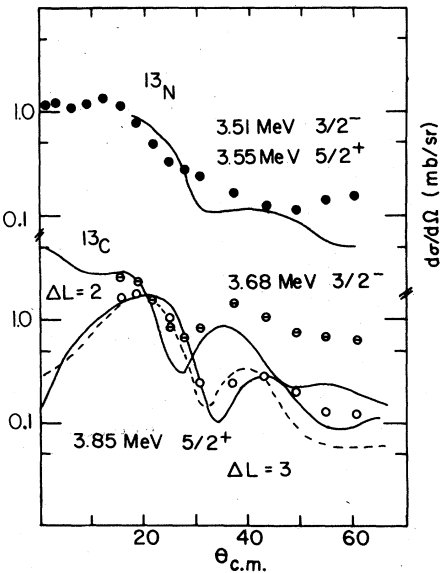


FIG. 8. Data for  $^3\text{He}$  scattering and charge exchange to the lowest  $\frac{3}{2}^-$  and  $\frac{5}{2}^+$  states are shown. The solid points are for the unresolved states in  $^{13}\text{N}$ . Collective  $\Delta L = 2$  and  $\Delta L = 3$  curves are shown for the 3.68 MeV  $\frac{3}{2}^-$  and 3.85 MeV  $\frac{5}{2}^+$  states of  $^{13}\text{C}$ . The broken curve compared to the 3.85 MeV data is a microscopic  $\Delta L = 3$  DWBA prediction. The solid curve through the  $^{13}\text{N}$  data is the shape of the sum of the  $^{13}\text{C}$  data, and is used to obtain the ratio of cross sections.

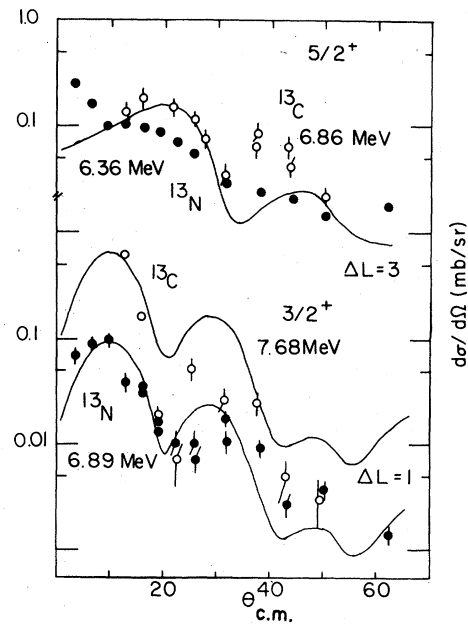


FIG. 9. Scattering and charge exchange  $^3\text{He}$  data for resolved  $\frac{3}{2}^+$  and  $\frac{5}{2}^+$  states in  $^{13}\text{C}$  and  $^{13}\text{N}$  are shown, with the  $^{13}\text{C}$  data as open circles. Collective DWBA predictions for  $\Delta L = 1$  and 3 are compared to the data.

study, so the  ${}^3\text{He}$  data are compared to a curve obtained as the sum of the 7.155 MeV  $\frac{7}{2}^+$  and 7.376 MeV  $\frac{5}{2}^-$  excitations in  ${}^{13}\text{N}$ . Collective DWBA fits to the  ${}^{13}\text{N}$  data are shown in Fig. 10, and the  $\beta$  values are listed in Table III. The ratio of 0.165 provides predictions of  $-0.44$  and  $-0.20$  for the pion asymmetry, compared to a measured value of  $-0.30 \pm 0.10$ .<sup>1</sup> This agreement may be fortuitous due to the unresolved natures of the data; three states are included in the pion data. The  ${}^4\text{He}$  data, shown in Fig. 7, cannot be used to further this analysis, since two states are unresolved in  ${}^{13}\text{C}$ .

#### F. The $\frac{9}{2}^+$ states

The most striking pion asymmetry is found to a peak at 9.5 MeV in  ${}^{13}\text{C}$ .<sup>1,2</sup> This state has been shown to have a spin of  $\frac{9}{2}^+$ .<sup>23</sup> The analog state in  ${}^{13}\text{N}$  is not resolved from a  $\frac{1}{2}^-$  state,<sup>25</sup> whose analog shows an asymmetry of opposite sign to the  $\frac{9}{2}^+$  transition in the pion data on  ${}^{13}\text{C}$ . The  ${}^3\text{He}$  data are shown in Fig. 11, compared to collective DWBA predictions for  ${}^{13}\text{C}$  and to the shape of the sum of the  $\frac{1}{2}^-$  and  $\frac{9}{2}^+$  states for  ${}^{13}\text{N}$ . The  $\beta$  strength parameters are listed in Table III.

To minimize the influence of the unresolved  $\frac{1}{2}^-$  state in  ${}^{13}\text{N}$ , the ratio of cross sections is taken at 12 deg, where the  $\Delta L = 0$  DWBA prediction has a minimum. This cross section ratio of  $2 \pm 0.2$  predicts a pion asymmetry of either  $-0.78$  or  $0.64$ , the latter result being in agreement with the pion data,<sup>1</sup> where a value of  $0.8 \pm 0.2$  is seen. The value

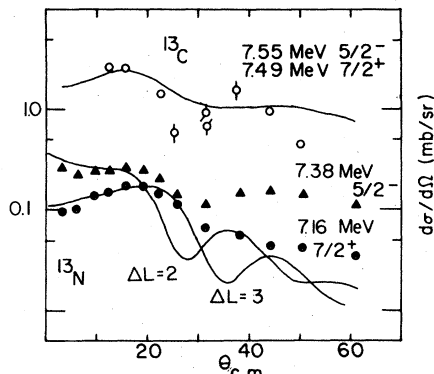


FIG. 10. Charge exchange data, shown as the solid points, for the 7.155 MeV  $\frac{7}{2}^+$  and 7.376 MeV  $\frac{5}{2}^-$  states of  ${}^{13}\text{N}$  are compared to  $\Delta L = 3$  and  $\Delta L = 2$  collective DWBA curves. The sum of these data provides the curve compared to the  ${}^3\text{He}$  scattering data to the unresolved analog states in  ${}^{13}\text{C}$ .

of  $\beta$  for the  ${}^{13}\text{N}$  data in Table III is for a fit including the unresolved  $\frac{1}{2}^-$  state.

The ratio of isovector to isoscalar reduced matrix elements is determined to be  $-4.2$  or  $0.72$  from the mass 3 data. This predicts an alpha yield either 0.7 or 5.0 times that of the  ${}^3\text{He}$  scattering. The DWBA corrected ratio of strengths is  $5.2 \pm 1.5$ , in agreement with the latter root. The  ${}^4\text{He}$  and  ${}^3\text{He}$  cross sections both have much less structure than predicted by the collective  $\Delta L = 5$  DWBA prediction.

#### G. Higher states

Further known states of  ${}^{13}\text{C}$  and  ${}^{13}\text{N}$  have been analyzed, and the  ${}^3\text{He}$  data are shown in Fig. 12, but for several cases the width of the states is such that states were not separated and no ratio data would be meaningful.

The  $\frac{3}{2}^-$  states listed<sup>18</sup> at 9.90 MeV in  ${}^{13}\text{C}$  and 9.48 MeV in  ${}^{13}\text{N}$  provide the data shown in Fig. 12. The collective  $\Delta L = 2$  DWBA fit to the  $({}^3\text{He}, t)$  data is consistent with the spin assignment, with  $\beta_2 = 0.020$ , but the scattering data show a completely different angular distribution, and no ratio can be obtained. The  ${}^{13}\text{C}$  state was too weakly excited by

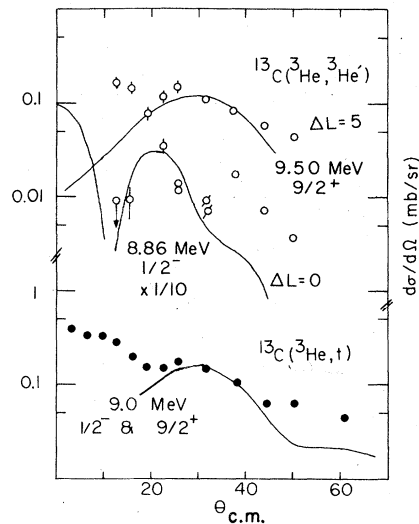


FIG. 11. Near 9 MeV of excitation in  ${}^{13}\text{C}$  there is a known  $\frac{1}{2}^-$  state, with data compared to a collective  $\Delta L = 0$  prediction, and a 9.498 MeV state now known to have a spin of  $\frac{9}{2}^+$ . A collective  $\Delta L = 5$  prediction is compared to the scattering data. These states are not resolved in the wide 9.0 MeV peak in  ${}^{13}\text{N}$ , but the similarity of shape to the  $\frac{9}{2}^+$  state in  ${}^{13}\text{N}$  indicates a small yield from the  $\frac{1}{2}^-$  level.

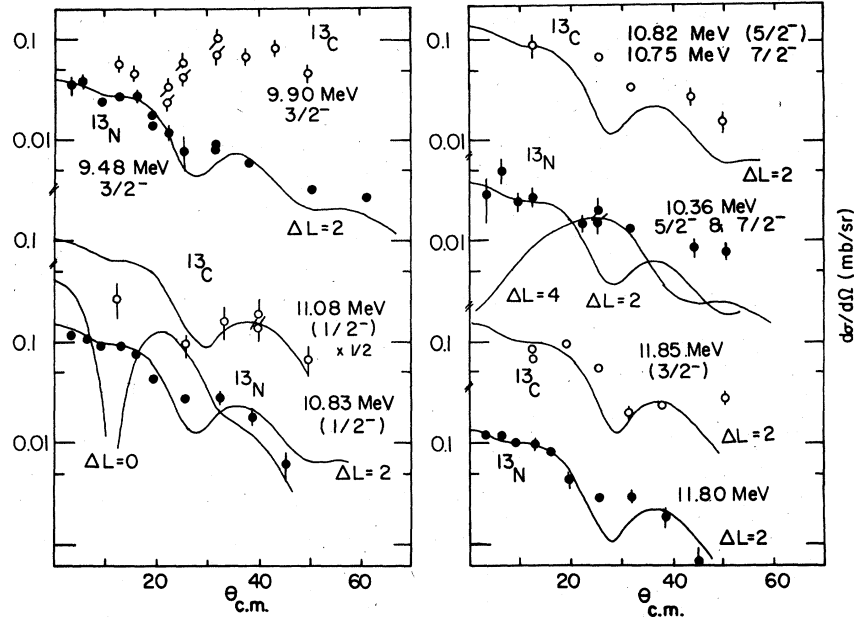


FIG. 12. Data, in some cases sparse, for  ${}^3\text{He}$  scattering and charge exchange to higher states in  ${}^{13}\text{C}$  and  ${}^{13}\text{N}$  are shown and compared to the appropriate DWBA collective predictions. Comparisons of these mirror transitions are discussed in the text. The solid data points are for  ${}^{13}\text{N}$  and the open points for  ${}^{13}\text{C}$  final states.

${}^4\text{He}$  scattering to be analyzed.

A doublet of  $\frac{5}{2}^-$  and  $\frac{7}{2}^-$  states is seen in both  ${}^{13}\text{C}$  and  ${}^{13}\text{N}$ , at 10.8 and 10.36 MeV.<sup>18</sup> The ( ${}^3\text{He}, t$ ) data are compared to collective DWBA predictions for  $\Delta L = 2$  and 4 in Fig. 12, with  $\beta_2 = 0.019$  and  $\beta_4 = 0.023$ . The cross section ratio of  $0.3 \pm 0.1$  provides ratios of matrix elements equal to  $-0.65$  and  $0.37$ . No pion data are reported for this doublet,<sup>1</sup> but asymmetries of  $-0.59$  and  $0.36$  are predicted.

A distinct  $\Delta L = 2$  shape is found in the  ${}^4\text{He}$  scattering data to the  $\frac{5}{2}^-$  and  $\frac{7}{2}^-$  states at 10.8 MeV, as seen in Fig. 7; this excitation is 26 times greater than that induced by  ${}^3\text{He}$  scattering. The  ${}^3\text{He}$  data provide ratios of matrix elements that predict  ${}^4\text{He}$  scattering either 1.1 or 3.2 times the  ${}^3\text{He}$  scattering strength.

The next clear pair of states are the 11.080 MeV ( $\frac{1}{2}^-$ ) state in  ${}^{13}\text{C}$  and the 10.833 MeV ( $\frac{1}{2}^-$ ) state in  ${}^{13}\text{N}$ . The ratio of the charge exchange to  ${}^3\text{He}$  scattering cross sections is 0.65, giving ratios of isovector to isoscalar transition matrix elements of  $-1.2$  and  $0.50$ . The 11.08 MeV state was not analyzed in the pion data.<sup>1,2</sup> The 10.83 MeV ( ${}^3\text{He}, t$ ) data are compared to  $\Delta L = 0$  and 2 collective DWBA predictions in Fig. 12. The failure of the  $\Delta L = 0$  fit indicates that either the tentative ( $\frac{1}{2}^-$ ) spin assignment<sup>18</sup> is in error or that an unex-

pected selection rule eliminates the  $\Delta L = 0$  cross section expected to dominate the excitation. A  $\Delta L = 2$  transition could include the transfer of a unit of spin to populate a  $\frac{1}{2}^-$  state.

The  ${}^4\text{He}$  scattering data to this 11.08 MeV state also proceeds by  $\Delta L = 2$ , as seen in Fig. 7. Since no spin transfer is expected for this scattering, final spins of  $\frac{3}{2}^-$  or  $\frac{5}{2}^-$  are inferred, and if in fact this state is analog to the 10.83 MeV level in  ${}^{13}\text{N}$ , the spin ( $\frac{1}{2}^-$ ) is in error. This 11.08 MeV state is excited 11 times more strongly by  ${}^4\text{He}$  scattering than by  ${}^3\text{He}$  excitation. Predictions of 0.71 and 4.0 are obtained for this ratio from the method of ratios of reduced matrix elements from  ${}^3\text{He}$  scattering and charge exchange.

Both the 10.8 and 11.08 MeV states are relatively even more strongly excited by  ${}^4\text{He}$  scattering than the large values predicted, but the large uncertainties for the weak  ${}^3\text{He}$  scattering may be noted from the data shown in Fig. 12.

The state near 12 MeV seen in the pion scattering<sup>1</sup> is possibly the 11.85 MeV ( $\frac{3}{2}^-$ ) (Ref. 18) level strongly seen in the present and earlier<sup>19</sup> work, with the analog at 11.878 MeV in  ${}^{13}\text{N}$ . The  ${}^3\text{He}$  data are shown in Fig. 12, but since several broad states<sup>18</sup> are not resolved in  ${}^{13}\text{N}$ , the scattering to charge exchange ratio of  $2.4 \pm 0.4$  may not be suitable for comparison to the pion data. Indeed, the predicted

pion asymmetries of  $-0.60$  and  $0.66$  do not agree with the small negative asymmetry  $-0.1 \pm 0.05$  observed.<sup>1</sup>

This  $11.85$  MeV state is strongly excited by  ${}^4\text{He}$  scattering, with the data and DWBA fit shown in Fig. 7. The ratio of  ${}^4\text{He}$  to  ${}^3\text{He}$  scattering cross sections is  $8.5$ , compared to predictions of  $0.10$  and  $6.3$  made from the  ${}^3\text{He}$  scattering and charge exchange. This preference for the negative square root solution does not agree with the pion data, where a large positive asymmetry is then predicted.

The  $({}^3\text{He}, t)$  data to the  $11.80$  MeV state of  ${}^{13}\text{N}$  show a nice  $\Delta L = 2$  angular distribution, but the sparse data for  ${}^3\text{He}$  scattering to the  $11.85$  MeV level in  ${}^{13}\text{C}$  indicates some contribution from a higher transfer (see Fig. 12). A poor  $\Delta L = 2$  fit is found for the  ${}^4\text{He}$  scattering to this level, as shown in Fig. 7. The pion scattering to this state, calibrated to be at  $11.82$  MeV, shows very similar magnitudes and identical shapes for both pion charge states.<sup>26</sup> A good fit to either a collective or a microscopic distorted-wave impulse approximation (DWIA) prediction for  $\Delta L = 3$  is found, as expected for a predicted but otherwise unknown pair of states with spins  $\frac{5}{2}^+$  and  $\frac{7}{2}^+$ .<sup>26</sup> The discrepancy between the pion asymmetry predicted and observed is thus probably due to the excitation of different states by the several reactions.

A state at  $16$  MeV nearly meets the pion asymmetry limit for a single proton excitation,<sup>1</sup> with  $A = -0.6 \pm 0.2$ . Data for the  $16.0 \pm 0.1$  MeV peak in  ${}^{13}\text{C}$  and the  $16.02$  MeV  $\frac{7}{2}^+$  state in  ${}^{13}\text{N}$  are shown in Fig. 13, compared to the  $\Delta L = 3$  DWBA curves. The ratio of  $1.4$  for the present cross sections provides predicted pion asymmetries of  $-0.97$  and  $+0.58$ , with the former result near agreement with the data. The uncertainties in the pion asymmetries predicted in this fashion will be discussed in Sec. VI.

The  ${}^4\text{He}$  scattering experiment found a very weak excitation of the  $16.0$  MeV peak, with  $\beta$  less than  $0.1$ , or less than  $2.6$  times the  ${}^3\text{He}$  yield. The predicted  ${}^4\text{He}$  strengths are  $0.33$  and  $5.0$  times the  ${}^3\text{He}$  strength. This result rules out the positive ratio of matrix elements, in agreement with the pion data, as shown in Table III.

#### H. $T = \frac{3}{2}$ states

The scattering and charge exchange cross sections to a  $T = \frac{3}{2}$  state are not as predicted by the equations of Sec. I, derived for  $T_i = T_f = \frac{1}{2}$ . After reduction in both the projectile and target isospin

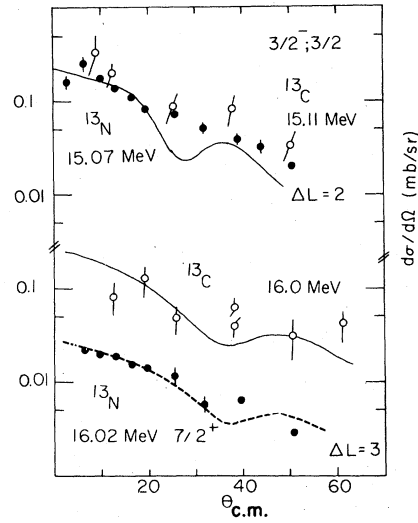


FIG. 13. Data for the  $T = \frac{3}{2}$  levels at  $15.11$  MeV in  ${}^{13}\text{C}$  and  $15.07$  MeV in  ${}^{13}\text{N}$  are expected to be equal. The results are shown and compared to a collective  $\Delta L = 2$  DWBA shape. Data for a  $16$  MeV pair are also shown. This is identified as a  $\frac{7}{2}^+$  state in  ${}^{13}\text{N}$  and compared to the collective  $\Delta L = 3$  DWBA curve.

projections, the strictly isovector excitations of the  $T = \frac{3}{2}$  states should be equal for the  ${}^3\text{He}$  scattering and  $({}^3\text{He}, t)$ . Data for the  $15.11$  MeV  $\frac{3}{2}^-$ ,  $T = \frac{3}{2}$  level in  ${}^{13}\text{C}$  and the  $\frac{3}{2}^-$ ,  $T = \frac{3}{2}$  level at  $15.07$  MeV in  ${}^{13}\text{N}$  are compared in Fig. 13 and, indeed, are found to be equal to within the limits of the sparse scattering data. A collective  $\Delta L = 2$  DWBA prediction is in agreement with the shape of these data.

Pion scattering to the  $15.1$  MeV  $T = \frac{3}{2}$  level in  ${}^{13}\text{C}$  has not been observed, but predictions in a shell model calculation<sup>16,27</sup> indicate equal  $\pi^+$  and  $\pi^-$  strengths, as expected from the present baryon data.

#### IV. DISTORTED-WAVE BORN APPROXIMATION AND COUPLED-CHANNEL BORN APPROXIMATION CALCULATIONS

Several of the states populated in the present work show distinct single-nucleon excitation in their pion asymmetries, and several have relatively high spins. These features should make possible a detailed description of the reaction mechanism responsible for their excitation, which in turn sheds light upon the modes of pionic excitation in the context of the present comparison.

The first  $\frac{7}{2}^+$  and  $\frac{9}{2}^+$  states are predicted<sup>28-30</sup> and observed<sup>23</sup> to be based on a  $d \frac{5}{2}$  nucleon coupled to the first  $2^+$  excited state of  ${}^{12}\text{C}$ . A prominent two-step path by the  $({}^3\text{He}, \alpha)p_{3/2}$  pickup to the

4.4 MeV state of  $^{12}\text{C}$ , followed by  $d \frac{5}{2}^-$  stripping by the  $(\alpha, t)$  or  $(\alpha, ^3\text{He})$  reactions, should be important for the  $^3\text{He}$  induced excitations. For that  $T = 0$  intermediate state, the predictions for  $^{13}\text{C}$  and  $^{13}\text{N}$  final states will be identical.

For computational simplicity the calculation was run for a  $0^+$  target through a  $\frac{3}{2}^-$  level in  $^{11}\text{C}$  to a final  $4^-$  state, using the CHUCK2 (Ref. 31) with a local, zero range pickup interaction. The  $(^3\text{He}, \alpha)$  data obtained with the auxiliary experiment using solid state detectors are compared to the prediction at the top of Fig. 14, with the prediction normalized to a total  $p_{3/2}$  spectroscopic factor of 4 divided equally into one each for the  $T = 0$  and  $1, 1^+$  and  $2^+$  states of  $^{12}\text{C}$ , as observed in the present work. The fit is not very good, but the magnitude is appropriate.

The stripping calculation for the second stage was performed in the strong coupling model,<sup>32</sup> as previously applied for the  $^{12}\text{C}(^3\text{He}, d)^{13}\text{N}$  reaction popu-

lating the same  $\frac{7}{2}^+$  and  $\frac{9}{2}^+$  levels.<sup>23</sup> Data for the 7.155 MeV  $\frac{7}{2}^+$  state in  $^{13}\text{N}$  are compared to the absolutely normalized prediction in Fig. 14. The agreement in magnitude is perfect, and the shape is fairly well reproduced. Although the analogous  $\frac{7}{2}^+$  level in  $^{13}\text{C}$  is not resolved in the present work, this agreement indicates the mechanism involved.

For the  $\frac{9}{2}^+$  state, it is the  $^{13}\text{C}$  that offers a certain singlet. The data and coupled-channel Born approximation (CCBA) predictions for the  $(^3\text{He}, \alpha)(\alpha, ^3\text{He})$  mechanism compared in Fig. 14 show a great discrepancy in shape and magnitude.

Also shown in Fig. 14 is a broken curve for sequential  $^3\text{He}$  inelastic scattering to the  $\frac{9}{2}^+$  state, using deformations  $\beta_2 = -0.6$  and  $\beta_3 = 0.5$ , with a weak coupling prediction for a  $\frac{9}{2}^+$  final state,

$$\frac{d\sigma}{d\Omega}(\frac{9}{2}^+) = \frac{10}{18} \frac{d\sigma}{d\Omega}(4^-),$$

since again a  $0^+$  target was used for the calculation. All scattering predictions used this weak coupling model. This comparison indicates that this may be an important process (also for the  $\frac{7}{2}^+$  state), but lack of a detailed model precludes a more precise statement. The parallel path, first through the  $3^-$  state, was not included, but could greatly increase the prediction.

This same sequential scattering prediction for the  $^4\text{He}$  scattering is compared to the  $\frac{9}{2}^+$  data as the broken curve in Fig. 7, divided by ten to compare with the data. More structure is predicted than is found, and the yield is not so large as predicted. The discrepancy in shape is much like that noted for the  $^3\text{He}$  scattering.

The strongest prediction for the two-step  $^3\text{He}$  excitation of the  $\frac{9}{2}^+$  state is by the  $(^3\text{He}, d)(d, ^3\text{He})$  [or  $(d, t)$ ] mechanism. Only  $3^-$  levels in  $^{14}\text{N}$  are eligible for the intermediate state, so the prediction, computed again for a  $0^+$  to  $4^-$  transition, was multiplied by  $\frac{1}{5}$  to account for the fraction of the predicted intermediate cross section actually observed to excite  $3^-$  states<sup>18</sup> and a factor of  $\frac{10}{34}$  for the fraction of second stages that could excite the  $\frac{9}{2}^+$  level. This is simply from  $2J_f + 1 = 10$  divided by the sum of statistical weights for all final states allowed for  $2^-$  and  $3^-$  intermediate state. This prediction, shown as the dotted line for the  $\frac{9}{2}^+$  data of Fig. 14, is still too high. The prediction has been divided by ten for the comparison. Although no detailed model has been used, this sequential nucleon transfer is certainly a very important mechanism for excitation of high spin states in  $^{13}\text{C}$  and  $^{13}\text{N}$ .

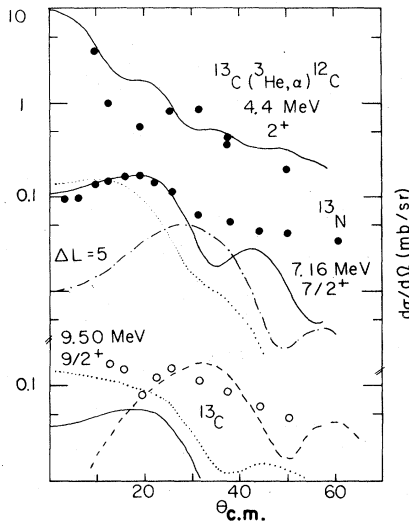


FIG. 14. At the top are shown  $(^3\text{He}, \alpha)$  data to the 4.4 MeV  $2^+$  state of  $^{12}\text{C}$  and a local, zero range DWBA prediction. Subsequent stripping on this  $2^+$  state, computed within the CCBA, provides the solid curve compared to the  $\frac{7}{2}^+$  data for  $^{13}\text{N}$ . There are no free parameters in this calculation, which fails for the  $^{13}\text{C} \frac{9}{2}^+$  data below, also shown by a solid curve. The dot-dash curve compared to the  $\frac{7}{2}^+$  data shows a  $\Delta L = 5$  tensor prediction, while the dotted curve shows a central  $\Delta L = 3$  prediction. The strengths are arbitrary in these calculations. The broken curve for the  $\frac{9}{2}^+$  state shows the results for sequential scattering by  $\Delta L = 2$  and  $\Delta L = 3$ . The dotted curve shows the  $(^3\text{He}, d)(d, ^3\text{He})$  prediction via  $3^-$  states in  $^{14}\text{N}$ , divided by ten for comparison to the data.

The  ${}^4\text{He}$  excitation of the  $\frac{9}{2}^+$  state by sequential stripping and pickup through levels in  ${}^{14}\text{N}$  was predicted in the same fashion. This mechanism could be one means of transferring spin in  ${}^4\text{He}$  scattering,<sup>33</sup> but the present prediction is orders of magnitude smaller than the data. This is as found for spin-flip scattering of  ${}^4\text{He}$  to the 12.7 MeV  $1^+$  state of  ${}^{12}\text{C}$ , where the data were stronger than any prediction.<sup>33</sup>

A direct, central  $\Delta L = 3$  promotion from the  $p_{\frac{1}{2}}$  into the  $d_{\frac{5}{2}}$  orbit could excite the  $\frac{7}{2}^+$ , but not the  $\frac{9}{2}^+$  states. The dotted curve compared to the  $\frac{7}{2}^+$  data for  $({}^3\text{He},t)$  in Fig. 14 shows the prediction, with  $V_T = 3.4$  MeV. The fit is poor. A tensor force inducing the same transition can provide  $\Delta L = 3$  or 5, with the  $\Delta L = 3$  prediction much smaller than that for  $\Delta L = 5$ . The dot-dashed curve compared to the  $\frac{7}{2}^+$  data, for a tensor force of range  $0.7 \text{ fm}^{-1}$  and  $V_T = 5.5$  MeV, can be added to the  $\Delta L = 3$  central prediction to account fairly well for the data. This shape also represents the structure in the  $\frac{9}{2}^+$  data near 35 degrees, with  $\Delta L = 5$  allowed for the tensor transition operator. Some  $\Delta L = 3$ ,  $\Delta S = 1$  strength could account for the smaller angle data for this  $\frac{9}{2}^+$  level.

It is evident from these comparisons that no single mechanism is required by the data. The  $\frac{7}{2}^+$   $({}^3\text{He},t)$  cross section can be represented by sequential nucleon transfer without free parameters, or by a sum of central and tensor direct excitations, with not unreasonable strengths. The sequential nucleon transfer predictions fail for the  $\frac{9}{2}^+$  state, which cannot be fit by a purely  $\Delta L = 5$  tensor prediction either. Sequential scattering through the large deformations known to be present near  ${}^{12}\text{C}$  are also important. Since all these scattering mechanisms provide predictions which must be added coherently, there is no reasonable way to combine them, and no simple conclusions can be drawn for the mechanism responsible for exciting these simple  $\frac{7}{2}^+$  and  $\frac{9}{2}^+$  states by either  ${}^3\text{He}$  or  ${}^4\text{He}$  excitation. The isospin ratios tested in this work, however, are not predicated upon a particular mechanism for the excitation.

## V. SUMMARY AND CONCLUSIONS

Application of the Wigner-Eckart theorem to the scattering amplitudes for baryonic scattering and charge exchange and for inelastic scattering of positive or negative pions provides independent means of obtaining the ratio of isovector to isoscalar re-

duced matrix elements between nuclear states of isospin  $\frac{1}{2}$ . This has been tested using the  $({}^3\text{He},t)$  and  $({}^3\text{He},{}^3\text{He}')$  reactions on  ${}^{13}\text{C}$ , with the ratio of matrix elements used to predict pion scattering charge asymmetries for a number of states. In all cases not obscured by unresolved multiplets one of the two allowed solutions is in agreement with the pion data. In many cases, these results are confirmed with inelastic alpha particle scattering.

The sensitivity of the predicted pion asymmetries to the accuracy of the present data is best illustrated in Fig. 15. Data from Ref. 1 and the present are shown in the boxes for the more securely known levels. It is seen that the larger asymmetries are well defined, and that the pure neutron excitation at the 3-3 resonance ( $A_\pi = +0.8$ ) requires a small  ${}^3\text{He}$  inelastic scattering yield, and the pure proton limit of  $A_\pi = -0.8$  may be obtained for a small charge exchange yield. These are just the effects expected in the  ${}^3\text{He}$  induced reactions for a sequential nucleon transfer with an intermediate deuteron, not an intermediate  ${}^4\text{He}$ .

The levels examined in  ${}^{13}\text{C}$  and  ${}^{13}\text{N}$  are mirrors, but are not completely identical due to differences in neutron and proton separation energies. The states compared are not even of the same width, with about 250 keV for the 9.0 MeV  $\frac{9}{2}^+$  level of  ${}^{13}\text{N}$  and 5 keV for the 9.5 MeV  $\frac{9}{2}^+$  level in  ${}^{13}\text{C}$ .<sup>18</sup> Nonetheless, the comparison to the pion data in Fig. 15 shows that the analysis appears valid.

The choice of solutions to compare in Fig. 15 may be determined by the alpha particle scattering. This is found to be correctly predicted for all of the single states analyzed, although the  ${}^4\text{He}$  data are not consistent with the  ${}^3\text{He}$  scattering and charge exchange analysis for several weaker states not observed in the pion scattering.

The comparison of the strictly isovector charge exchange and strictly isoscalar  ${}^4\text{He}$  scattering is shown in Fig. 16, where the sensitivity to the uncertainties may be noted. For the states shown, these data are consistent with the simple equations of Sec. I, even though the results are compared via collective DWBA predictions.

There is a single comparison possible for the ratios of electromagnetic transition rates in  $A = 13$ , and this is found to be consistent with the  ${}^3\text{He}$ ,  ${}^4\text{He}$ , and pion data, all related simply through the use of the Wigner-Eckart theorem on the isospin projection variables offered by the several projectiles.

The equation in Sec. I for the pion ratios includes the 3-3 resonance in that an intermediate isobar is included. This form provides nine for the  $\pi^-$  to  $\pi^+$

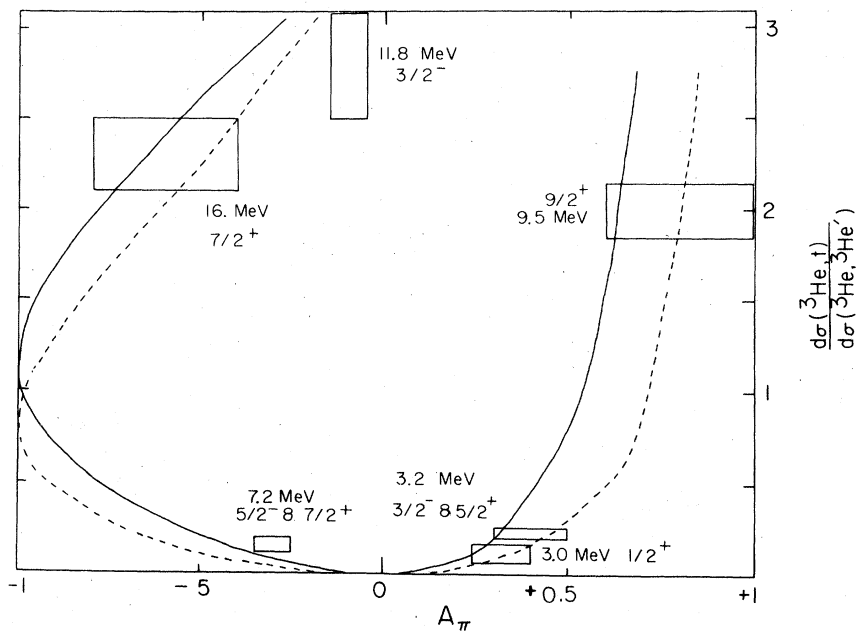


FIG. 15. Ratios of  $(^3\text{He},t)$  to  $(^3\text{He},^3\text{He}')$  cross sections on  $^{13}\text{C}$  to several final states are plotted with pion asymmetry data to provide the boxes, given the experimental uncertainties. The solid curve shows the expected relation between these data through the Wigner-Eckart theorem for a model incorporating the 3-3 resonance. A one-step model for the pion scattering provides the broken curve.

ratio of cross sections for a single-neutron excitation. This explicit model can be tested by using the present scattering and charge exchange data to predict the pion asymmetry for another pion scattering model.<sup>5</sup> This mechanism has no explicit recognition of the 3-3 resonance, and only a single pion-nucleon vertex is reduced. In this process the ratio

of cross sections is

$$\frac{d\sigma(\pi^-)}{d\sigma(\pi^+)} = \left| \frac{P_1 + \sqrt{2}P_0}{P_1 - \sqrt{2}P_0} \right|^2$$

The predicted asymmetries are graphed in Fig. 15 as the broken curves. These are similar enough to the solid curves for the resonant two step model that the present data and those of Ref. 1 are not able to select one or the other, although a superior fit is seen for the broken curve. This distinction would be a worthwhile goal for more precise experiments.

For a complex nucleus the 3-3 resonance is still observed in pion total cross sections, but is broadened.<sup>34</sup> The total cross sections for  $\pi^+$  and  $\pi^-$  also become more nearly equal. These features imply a more nearly equal decomposition into pion-nucleon channels of both  $T = \frac{1}{2}$  and  $\frac{3}{2}$ , as in the equation above. The shift observed from the solid curve in Fig. 15 towards the broken curve is consistent with this expectation.

No systematic choice of a preferred root is indicated by the parity of the transition, and no attempt is made to compute the relative signs of isoscalar and isovector amplitudes in this work. This calculation is given for pion scattering in Refs. 12 and 16.

Higher resolution pion scattering data would be

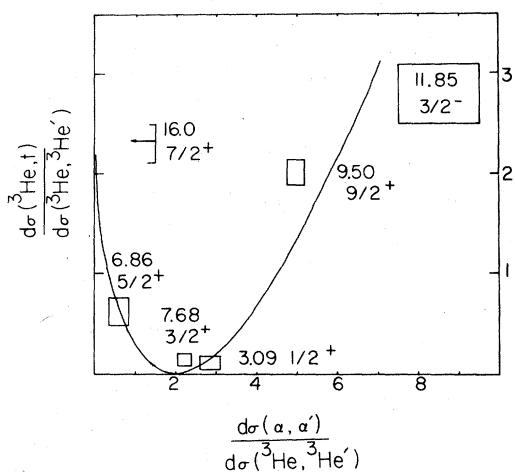


FIG. 16. Ratios of  $(^3\text{He},t)$  to  $(^3\text{He},^3\text{He}')$  cross sections on  $^{13}\text{C}$  are compared to the  $(^4\text{He},^4\text{He}')$  to  $(^3\text{He},^3\text{He}')$  ratio for several states. The solid curve shows the relation expected through the equations in the text.

especially valuable for the 7.68 MeV  $\frac{3}{2}^+$  state, with a simple neutron decay observed in photonuclear work<sup>35</sup> and included in photonuclear calculations,<sup>36</sup> and to the 6.86 MeV  $\frac{5}{2}^+$  state, with an allowed solution for an asymmetry of  $A_\pi = -1$ , corresponding to a single proton excitation. The single-particle  $d \frac{5}{2}$  state in  $A = 13$  is not this level, but the very strong state at 3.85 MeV,<sup>23</sup> which provides an asymmetry nearer the single-neutron limit,  $A_\pi = +0.4$ .<sup>1</sup>

The good success noted for the few available comparisons of pion asymmetries, mirror gamma decay lifetimes,<sup>4,5</sup> and hadronic scattering and charge exchange indicate that a surprisingly simple isospin dependence relates these data, and that the isovector to isoscalar transition amplitude may be obtained by any such measurements, at least on light nuclei. This sensitive interference effect provides a new testing ground for nuclear models previously examined largely by beta decay, and by gamma decays of analog states. It has been shown that these results are highly sensitive to the structure of the states.<sup>37</sup>

No attempt has been made in the work to use es-

tablished wave functions to predict the ratio  $M_1/M_0$  or any absolute cross sections, nor have attempts been made to explain the ratios observed. We have, however, demonstrated that such information may be consistently obtained from a number of experimental methods through very simple relations. The reason for these simple successes is worthy of further investigation. One common feature to be noted for the hadronic probes of this work is their short mean free path within the nucleus. This feature perhaps allows the projectile dependence, with different complexities of dynamics and interactions, to cancel, leaving only the common sensitivity to the nuclear transition. A comparison of  $(pp')$  and  $(p,n)$  data, with less dominant strong absorption, may not find the same results.

#### ACKNOWLEDGMENTS

We wish to thank P. A. Smith and J. J. Hamill for aid in obtaining and reducing the data, and E. Siciliano for valuable discussions. The assistance of D. Dehnhard in the experiment and analysis is gratefully acknowledged. This work was supported in part by the U. S. Department of Energy.

- 
- <sup>1</sup>D. Dehnhard *et al.*, Phys. Rev. Lett. **43**, 1091 (1979).  
<sup>2</sup>E. Schwartz *et al.*, Phys. Rev. Lett. **43**, 1578 (1979).  
<sup>3</sup>H. A. Thiessen, Nucl. Phys. **A355**, 329 (1980).  
<sup>4</sup>A. M. Bernstein, V. R. Brown, and V. A. Madsen, Phys. Rev. Lett. **42**, 425 (1979).  
<sup>5</sup>R. J. Peterson, Nucl. Phys. **A335**, 365 (1980).  
<sup>6</sup>C. A. Wiedner *et al.*, Phys. Lett. **97B**, 371 (1980).  
<sup>7</sup>V. A. Madsen, V. R. Brown, and J. D. Anderson, Phys. Rev. C **12**, 1205 (1975).  
<sup>8</sup>D. E. Bainum *et al.*, Phys. Rev. Lett. **39**, 443 (1977).  
<sup>9</sup>C. L. Morris, Phys. Rev. C **13**, 1755 (1976).  
<sup>10</sup>D. Dehnhard *et al.* (unpublished).  
<sup>11</sup>A. M. Bernstein, Phys. Lett. **29B**, 335 (1969).  
<sup>12</sup>B. A. Brown and B. H. Wildenthal, Phys. Rev. C **21**, 2107 (1980).  
<sup>13</sup>A. Bohr and B. R. Mottelson, *Nuclear Structure* (Benjamin, New York, 1975), Vol. 2, p. 137.  
<sup>14</sup>A. de Shalit and I. Talmi, *Nuclear Shell Theory* (Academic, New York, 1963).  
<sup>15</sup>J. P. Schiffer, Bull. Am. Phys. Soc. **20**, 663 (1975).  
<sup>16</sup>T. S. H. Lee and R. D. Lawson, Phys. Rev. C **21**, 679 (1980).  
<sup>17</sup>B. W. Ridley *et al.*, Nucl. Instrum. Methods **130**, 79 (1975).  
<sup>18</sup>F. Ajzenberg-Selove, Nucl. Phys. **A268**, 1 (1978).  
<sup>19</sup>G. C. Ball and J. Cerny, Phys. Rev. **177**, 1466 (1968).  
<sup>20</sup>R. J. Peterson and J. J. Hamill (unpublished).  
<sup>21</sup>H. J. Trost *et al.*, Nucl. Phys. **A337**, 377 (1980).  
<sup>22</sup>P. Gaillard *et al.*, Nucl. Phys. **A131**, 353 (1969).  
<sup>23</sup>R. J. Peterson and J. J. Hamill, Phys. Rev. C **22**, 2282 (1980).  
<sup>24</sup>DWUCK4, a distorted wave Born approximation written by P. D. Kunz, University of Colorado (unpublished).  
<sup>25</sup>C. H. Holbrow, H. G. Bingham, R. Middleton, and J. D. Garrett, Phys. Rev. C **9**, 902 (1974).  
<sup>26</sup>S. Seestrom-Morris, Ph.D. thesis, University of Minnesota, 1981 (unpublished).  
<sup>27</sup>T. S. H. Lee and D. Kurath, Phys. Rev. C **21**, 293 (1980).  
<sup>28</sup>T. Sebe, Prog. Theo. Phys. **30**, 290 (1963).  
<sup>29</sup>J. L. Norton, Ph.D. thesis, University of Kansas, 1969 (unpublished); J. L. Norton and P. Goldhammer, Nucl. Phys. **A165**, 33 (1971).  
<sup>30</sup>H. U. Jager, H. P. Kissener, and R. A. Eramzhian, Nucl. Phys. **A171**, 25 (1971).  
<sup>31</sup>P. D. Kunz, University of Colorado (unpublished).  
<sup>32</sup>G. R. Satchler, Ann. Phys. (N.Y.) **3**, 275 (1958).  
<sup>33</sup>F. E. Cecil and R. J. Peterson, Phys. Lett. **56B**, 335 (1975).  
<sup>34</sup>A. S. Carroll *et al.*, Phys. Rev. C **14**, 635 (1976); E. Oset and W. Weise, Phys. Lett. **94B**, 19 (1980).  
<sup>35</sup>R. J. Holt *et al.*, Phys. Rev. C **21**, 1699 (1980).  
<sup>36</sup>H. R. Kissener, A. Asward, R. A. Eramzhian, and H. U. Jager, Nucl. Phys. **A219**, 601 (1974).  
<sup>37</sup>E. Osnes and C. S. Arke, Nucl. Phys. **A154**, 331 (1970).